J. Fluid Mech. (1988), *vol.* 196, *pp.* 323–344
Printed in Great Britain

The nonlinear breakup of a magnetic layer: instability to interchange modes

By F. CATTANEO AND D. W. HUGHES†
Joint Institute for Laboratory Astrophysics, University of Colorado, Boulder, CO 80309, USA

(Received 3 September 1987)

Motivated by considerations of the solar toroidal magnetic field we have studied the behaviour of a layer of uniform magnetic field embedded in a convectively stable atmosphere. Since the field can support extra mass, such a configuration is top-heavy and thus instabilities of the Rayleigh–Taylor type can occur. For both static and rotating basic states we have followed the evolution of the interchange modes (no bending of the field lines) by integrating numerically the nonlinear compressible MHD equations. The initial Rayleigh–Taylor instability of the magnetic field gives rise to strong shearing motions, thereby exciting secondary Kelvin–Helmholtz instabilities which wrap the gas into regions of intense vorticity. The subsequent motions are determined primarily by the strong interactions between vortices which are responsible for the rapid disruption of the magnetic layer.

1. Introduction

The appearance on the solar surface of bipolar magnetic regions, such as sunspots, aligned roughly parallel with the equator, is a consequence of the emergence of a strong, underlying toroidal magnetic field. Detailed observations over the past three hundred years have revealed the cyclic nature of sunspots. With a period of approximately eleven years the latitude at which the spots appear drifts from about 40° on either side of the equator to about 5° – a new cycle then restarts at high latitudes with a change in the polarity of the toroidal field. Of course, sunspots and other magnetic regions are just surface manifestations of an underlying complicated series of events taking place within the sun involving the regeneration of magnetic flux and its subsequent escape to the surface. The work described in this paper deals primarily with the latter phenomenon (the escape) but, as described below, was motivated also by considerations of the former (the regeneration mechanism).

It is widely believed that the sun's magnetic field is regenerated by some sort of $\alpha\omega$ dynamo mechanism involving a flow with net helicity, in order to generate a poloidal field from a toroidal field (the α-effect), and also differential rotation, ω, to carry out the reverse process. Solving the full dynamo problem is a task of considerable difficulty since it involves obtaining self-consistent solutions to both the momentum equation and the magnetic-induction equation. Consequently most progress has been made on the so-called kinematic dynamo problem in which the aim is to find a flow which, from the induction equation, will amplify the magnetic field – however, the flow and the resulting magnetic field are *not* constrained by the momentum equation. In particular, in kinematic dynamo models both α and ω are essentially free parameters and, by a judicious choice of these, a good agreement may

† Present address: Department of Applied Mathematics and Theoretical Physics, University of Cambridge, Silver Street, Cambridge CB3 9EW, U.K.

be reached with the observed solar field (see, for example, Roberts & Stix 1972; Yoshimura 1975). The most obvious site for solar dynamo action is the convection zone since therein is differential rotation (probably with both radius and latitude), as well as cyclonic convection leading to a net helicity. However, despite the convection zone possessing the two necessary ingredients for an $\alpha\omega$ dynamo, there are two major problems associated with the regeneration of magnetic fields within this region.

The most significant concerns the difficulty of keeping magnetic flux in the convection zone for periods comparable with that on which the field is regenerated, namely several years. Calculations of isolated flux tubes rising through the convection zone, in which the superadiabatic stratification is treated simply as a parameter of the problem, predict that magnetic flux will be carried from the bottom of the convection zone to the solar surface in only a few weeks (Parker 1975; Moreno-Insertis 1983, 1986). Such models are, however, a tremendous simplification since they neglect all interactions between the turbulent gas and the magnetic field. In reality the magnetic field is probably closely tied to the convection and, as a consequence, some of the field will be brought rapidly to the surface whereas some may be pushed to the base of the convection zone by concerted downward motions. Nevertheless, the fact remains that even with this more complicated picture magnetic flux may be expelled from the interior of the convection zone on a convective timescale ($\sim$ 1 month). The second major problem of a convection-zone dynamo concerns solutions which have recently been obtained to the dynamic (as opposed to kinematic) dynamo problem. With the advent of larger and faster computers in the past few years it has become possible to obtain self-consistent solutions to both the momentum and magnetic-induction equations (Gilman & Miller 1981; Gilman 1983; Glatzmaier 1985*a*, *b*). In the convection-zone dynamo models of Gilman and Glatzmaier, and in sharp contrast to kinematic dynamo models, α and ω are *not* free parameters but instead are determined by the dynamically consistent flow. What is found is that for surface differential rotation profiles that match the sun (i.e. with an equatorward acceleration) the resulting α and ω are such as to cause a migration of the toroidal field not towards the equator as observed on the sun, but instead towards the poles.

These two difficulties with a standard convection-zone dynamo have led to alternative theories and, in particular, it has been suggested (e.g. Spiegel & Weiss 1980; van Ballegooijen 1982) that the bulk of the toroidal magnetic field may be stored below the convection zone proper, in the convective overshoot zone. (Layzer, Rosner & Doyle 1979 have also suggested the presence of a magnetic field in the overshoot region although their idea of a fossil field leaking out from the radiative interior is very different to the dynamo process outlined above.) Such a location is favourable in two respects. The first is that in the models of Glatzmaier (1985*a*, *b*), which have a stably stratified region below the convection zone, there is a change in the sign of the helicity in this stable region which may lead to an equatorward propagation of the toroidal field. The second, and more compelling, reason is that the overshoot region is convectively stable and is therefore more suitable for confining the magnetic field. It was this aspect of the problem that provided the motivation for the work described in this paper; in particular we were interested in the behaviour of a magnetic field in a convectively stable region, whether it could escape and, if so, what form did this escape take. One of our hopes was that our calculations would provide a clue as to the nature of the magnetic field within the sun and would shed some light on the 'flux tubes versus diffuse fields' controversy. The magnetic field within the sun is typically treated in one of two ways – either as individual flux tubes

existing in a field-free atmosphere or as a diffuse field existing everywhere. Each of these treatments would appear to have its domain of validity – isolated flux tubes are indeed seen at the solar surface whereas deeper in the sun it seems more likely to us that any field produced by dynamo action will be of a more diffuse nature. Thus one of our aims was to study the formation of isolated flux tubes from the nonlinear disruption of a continuous magnetic layer.

The model we have studied, which is described in detail in §2, has, as its initial state, a uniform horizontal magnetic field embedded in a convectively stable atmosphere. The temperature and total (gas + magnetic) pressure are everywhere continuous, thereby causing a jump in the density at the interfaces of the magnetic field. In particular, at the upper surface of the field, heavier (non-magnetic) gas is being supported by lighter (magnetic) gas and thus instabilities of the Rayleigh–Taylor type can ensue.

Although we believe our work is the first in attacking the fully nonlinear development of compressible Rayleigh–Taylor instabilities driven by a magnetic field it is related, obviously, to studies of other Rayleigh–Taylor instabilities as well as, to a lesser extent, to investigations of magnetic buoyancy instabilities resulting from a vertical gradient in a continuously stratified horizontal magnetic field. What may be termed the 'classical' Rayleigh–Taylor instability, resulting from the acceleration of a heavy liquid into a lighter one, was conceived by Rayleigh (1883) and Taylor (1950) who both considered the linear theory of incompressible flows. The nonlinear development of the instability has been studied numerically by Daly (1967, 1969), Baker, Meiron & Orszag (1980) and Menikoff & Zemach (1983), for incompressible flows, and by Wang & Nepveu (1983), who incorporated the effects of compressibility. The effects of magnetic fields were included by Kruskal & Schwarzschild (1954) who investigated the linear instabilities of a plasma supported above a vacuum by a horizontal magnetic field. Although differing from Rayleigh–Taylor instabilities in not being driven by a discontinuity in the density profile, magnetic buoyancy instabilities arising from a vertical gradient in a horizontal field are related in that typically they also result from a release of gravitational potential energy made available by the magnetic field. Such instabilities have been studied in detail in the linear regime (Newcomb 1961; Parker 1966; Schubert 1968; Gilman 1970; Roberts & Stewartson 1977; Acheson 1978, 1979; Acheson & Gibbons 1978; Schmitt & Rosner 1983; Hughes 1985*a*, *b*; Hughes & Cattaneo 1987) and have also been investigated for finite-amplitude disturbances (Hughes 1987).

Another seemingly related problem, but one which actually turns out to have quite different properties, is that of the stability of an isolated flux tube (Spruit & van Ballegooijen 1982). Whereas a flux tube in static equilibrium must necessarily be cooler than the adjacent non-magnetic gas, the equilibrium of a magnetic layer (which is independent of the horizontal direction) imposes no such restriction on the temperature of the magnetic region. This important difference in the initial states of these two models leads to their having qualitatively different stability features – we shall elaborate on this in §3.1.

When studying any complex physical process it is always beneficial to start off with a relatively simple problem. For this reason, and also to facilitate the computation, we decided initially to consider two-dimensional disturbances. It is however important to give some thoughts as to what are the key modes in three dimensions. Our preliminary linear calculations suggest that the most rapidly growing three-dimensional mode has a long wavelength in the direction of the

imposed field and that, in the limit of this wavelength becoming infinite (and in the absence of rapid rotation), the resulting mode is a pure interchange with straight field lines and motion confined to the plane perpendicular to the magnetic field. Such behaviour is in keeping with other interfacial instabilities (see, for example, Kruskal & Schwarzschild 1954) but is rather different to that of the magnetic buoyancy instabilities of a smoothly varying field in which long-wavelength instabilities can tend to a purely horizontal flow in the limit – these latter modes do not appear to be of importance in interfacial instabilities. In two dimensions we found that undulatory modes, with motion along the field and in the vertical direction, were always stable due to the inhibiting amount of compressive work involved. Indeed, as discussed in detail by Hughes & Cattaneo (1987), this stabilizing feature is present even for magnetic buoyancy instabilities when undulatory modes *can* be important. Consequently in this paper we shall deal only with the interchange modes. In the light of the above comments on the dominant modes in three dimensions such a study is obviously of great relevance. The nonlinear evolution of the static initial state is considered in §3, the effects of uniform rotation are incorporated in §4.

Since we are interested not just in the early stages of the instability, but also in the long-term morphology of the magnetic field, we have integrated the governing equations for many timesteps, until virtually all of the energy has been dissipated. By so doing we have discovered the interesting feature that there are two distinct stages to the magnetic Rayleigh–Taylor instability. In the first, a magnetic field embedded in a convectively stable atmosphere becomes unstable to interchange modes and, as illustrated by the colour figures of §§3 and 4, the rising field forms the mushroom-shaped structures characteristic of Rayleigh–Taylor instabilities induced by only a small jump in the density (see, for instance, Daly 1967). Associated with the wings of the mushrooms are regions of intense vorticity and, in the second stage, when most of the available potential energy has been released, it is the vorticity distribution that plays a key role in the subsequent evolution of the layer. Indeed, somewhat surprisingly, certain interactions between vortex pairs are strong enough to prevent the escape of small pockets of high magnetic-field strength even though such regions are lighter than their surroundings.

2. Mathematical formulation

2.1. *The equations*

To model the instabilities of a magnetic field in the convective overshoot zone we considered an initial state consisting of a region of uniform horizontal magnetic field embedded in a field-free, convectively stable atmosphere. This of course is not a true equilibrium since, for any finite value of the magnetic diffusivity η, the magnetic diffusion equation ($\eta\nabla^2\boldsymbol{B} = 0$) is not satisfied across the interfaces of the magnetic field. However, this is not a serious problem provided that the instabilities grow on a timescale that is much shorter than that on which the field diffuses appreciably – this may be checked *a posteriori* and, fortunately, does indeed turn out to be true.

Our computational domain is between $z = 0$ (top) and $z = d$ (bottom). Initially the atmosphere is piecewise polytropic with a temperature distribution of the form $T = T_0 + \Delta z$ and a uniform horizontal magnetic field $B_0\hat{\boldsymbol{y}}$ confined to the region $z_1 < z < z_2$. The total (gas + magnetic) pressure is everywhere continuous, thereby giving rise to a density distribution as sketched in figure 1.

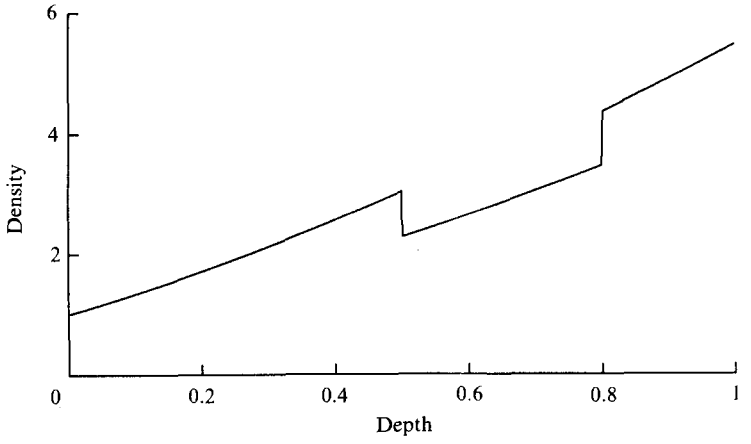

FIGURE 1. The density of the initial state as a function of depth. $m = 1.6$, $\theta = 2$, $\beta = 1$, $z_1 = 0.5$, $z_2 = 0.8$

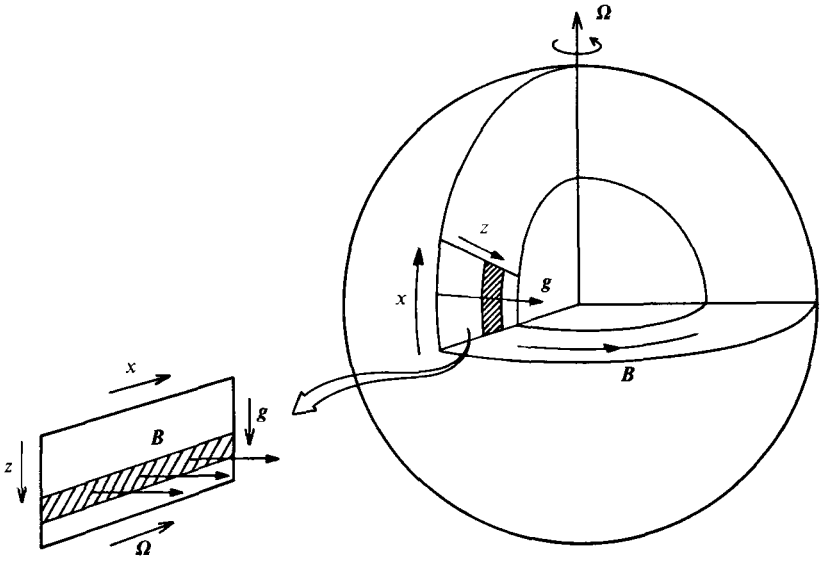

FIGURE 2. Schematic representation of the computational domain. The shaded region depicts the undisturbed magnetic layer.

For reasons explained in the introduction we shall concentrate only on interchange modes in this paper. All variables are independent of y and, in the absence of rotation, the fluid flow is in the (x, z)-plane only, perpendicular to the magnetic field $B\hat{\boldsymbol{y}}$. Our computational domain may then be thought of as a meridional slice near the equator with a toroidal field and with axisymmetric flows (see figure 2). To simplify the problem, the thermal conductivity K, the shear viscosity μ and the magnetic diffusivity η are assumed to be constants; furthermore the plasma obeys the perfect-gas law with constant specific heats. By choosing the layer depth d and the sound crossing time $d/(RT_0)^{\frac{1}{2}}$ as the units of length and time

respectively (R being the gas constant) the evolution equations can be expressed in dimensionless form as follows:

$$p = \rho T, \tag{2.1}$$

$$\partial_t \rho + \boldsymbol{\nabla} \cdot \rho \boldsymbol{u} = 0, \tag{2.2}$$

$$\partial_t B + \boldsymbol{\nabla} \cdot (B\boldsymbol{u}) = \tau C_k \nabla^2 B, \tag{2.3}$$

$$\partial_t \rho \boldsymbol{u} + \boldsymbol{\nabla} \cdot \rho \boldsymbol{u}\boldsymbol{u} = -\boldsymbol{\nabla}\left(p + \frac{B^2}{2\beta}\right) + \theta(m+1)\rho \hat{\boldsymbol{z}} + C_k \sigma(\nabla^2 \boldsymbol{u} + \tfrac{1}{3}\boldsymbol{\nabla}(\boldsymbol{\nabla} \cdot \boldsymbol{u})), \tag{2.4}$$

$$\rho(\partial_t T + \boldsymbol{u} \cdot \boldsymbol{\nabla} T) + (\gamma - 1) p \boldsymbol{\nabla} \cdot \boldsymbol{u} = \gamma C_k \nabla^2 T + (\gamma - 1) C_k (\sigma \phi_{ij} \partial_i u_j + \tau (\boldsymbol{\nabla} B)^2 / \beta), \tag{2.5}$$

where $\phi_{ij} = \partial_i u_j + \partial_j u_i - \frac{2}{3}\delta_{ij} \boldsymbol{\nabla} \cdot \boldsymbol{u}$.
The six dimensionless parameters are defined by:

$$\sigma = \frac{\mu C_p}{K}, \quad \tau = \frac{\eta \rho_0 C_p}{K}, \quad \beta = \frac{\mu_0 p_0}{B_0^2},$$

$$m = \left(\frac{g}{R\Delta} - 1\right), \quad \theta = \frac{\Delta d}{T_0}, \quad C_k = \frac{K}{\rho_0 C_p d (RT_0)^{\frac{1}{2}}},$$

where p_0 and ρ_0 are, respectively, the values of the pressure and density at $z = 0$, μ_0 is the magnetic permeability and C_p is the specific heat at constant pressure. It should be noted that this β is a somewhat strange parameter since it is a comparison of the gas presure at the top of the domain to the magnetic pressure in the region of uniform field. We define a local value of β by $\beta_\ell = \beta(1 + z_1 \theta)^{m+1}$, the ratio of the gas pressure in the field-free gas immediately above the interface to the magnetic pressure.

The formulation of the problem is completed by imposing boundary conditions at the top and bottom and by requiring that all variables be periodic in the horizontal direction. In the physical context of the solar overshoot zone it is unclear exactly what the boundary conditions should be and, in any case, it is certainly unrealistic to apply complicated conditions to our highly idealized model. Thus, with the understanding that any instability ceases to be of interest once the influence of the boundaries is significant, we decided on the following simple boundary conditions for the horizontal surfaces:

$$T = 1 \quad \text{at} \quad z = 0, \qquad T = 1 + \theta \quad \text{at} \quad z = 1;$$

$$w = \partial_z u = \partial_z B = 0 \quad \text{at} \quad z = 0, 1.$$

In §4 we incorporate the effects of uniform rotation about an axis orthogonal to both $\boldsymbol{B}$ and $\boldsymbol{g}$. The momentum equation (2.4) is amended by the inclusion of the Coriolis term $2\boldsymbol{\Omega} \times \rho \boldsymbol{u}$ on the left-hand side; the centrifugal acceleration is neglected since in the solar context it is several orders of magnitude smaller than that due to gravity. The remaining equations are unaltered in a rotating frame of reference. Rotation induces a flow in the y-direction, v say, although v is still independent of y. On the horizontal boundaries ($z = 0, 1$) v is assumed to satisfy $\partial_z v = 0$.

2.2. *Numerical techniques*

2.2.1. *The linear equations*

Although our primary interest lies in the fully nonlinear development of the instabilities, linear theory has an important role to play in determining the variation

of the onset of instability with the parameters of the problem. In our numerical treatment of the nonlinear problem (see §3.2) the magnetic field initially has a 'top hat' profile but this is smeared out immediately to give a profile that is continuous but has very steep gradients at $z = z_1, z_2$. Consequently, in order to obtain a reasonable agreement between our linear results and the early stages of the fully nonlinear evolution, we decided to adopt such a continuous field as the initial state for our linear stability analysis. We opted for a field variation of the form $\frac{1}{2}\{\tanh(30(z-z_1)) - \tanh(30(z-z_2))\}$ although, provided that the field is approximately uniform between z_1 and z_2 and dies off rapidly elsewhere, its exact form is not important.

Let the linear perturbation of the magnetic field be expressed as $\delta\boldsymbol{B} = (0, b, 0)$, the velocity as $\boldsymbol{u} = (u, 0, w)$ and the perturbations of the pressure, density and temperature as δp, $\delta\rho$ and δT respectively. (It is worth noting that with an initial field as described above the perturbed field b is everywhere non-zero, in contrast to the perturbation of a discontinuous field.) The linearized versions of (2.1)–(2.5) are separable in x and t with u proportional to $\sin lx\, \mathrm{e}^{st}$ and all other variables proportional to $\cos lx\, \mathrm{e}^{st}$. After eliminating δp by means of the perfect-gas equation (2.1) the linear evolution equations (in the absence of rotation) take the form

$$s\boldsymbol{\phi} = \mathbf{L}\boldsymbol{\phi}, \tag{2.6}$$

where $\boldsymbol{\phi} = (\delta T, u, w, b, \delta\rho)^{\mathrm{T}}$ is the solution vector and $\mathbf{L}$ is a 5×5 matrix whose elements are linear differential operators in z. (When the effects of rotation are included $\boldsymbol{\phi}$ contains the extra element v (proportional to $\cos lx\, \mathrm{e}^{st}$) and $\mathbf{L}$ becomes a 6×6 matrix.) To solve (2.6) the interval $0 < z < 1$ is divided into n equally spaced points (typically 40) and the differential operators replaced by fourth-order finite differences. Equation (2.6) is then turned into an eigenvalue problem for a $5n\times5n$ matrix, $\mathbf{L}_*$ say. All of the eigenvalues and eigenvectors of $\mathbf{L}_*$ were determined by an NCAR library routine (EIGRG1). Having found the eigenvalues and eigenvectors of interest these were then calculated much more accurately by the method of inverse iteration (see, for example, Stoer & Bulirsch 1980), using considerably more mesh points (typically 100).

2.2.2. *The nonlinear equations*

The study of the fully nonlinear regime was achieved by integrating the equations in time. At each iteration the updating of the five (with no rotation) field variables requires the evaluation of both temporal and spatial derivatives. The timestepping scheme is best described in terms of the following simple advection–diffusion equation:

$$\partial_t X = -\boldsymbol{u}\cdot\boldsymbol{\nabla}X + \kappa\nabla^2 X = F(X) + D(X), \tag{2.7}$$

where $F(X)$ and $D(X)$ represent the hyperbolic and parabolic terms respectively. Different techniques were used for these two terms.

An explicit two-level scheme was employed to treat the advective term; a predictor step which calculates an approximate value of X at the new time is followed by a corrector step which improves the accuracy of the estimate. This technique, which is referred to as a partially corrected Adams–Bashforth scheme (see Gazdag 1976), applied to (2.7) yields

$$\left.\begin{aligned} \tilde{X}^{n+1} &= X^n + \tfrac{1}{2}\delta t[3F(\tilde{X}^n) - F(\tilde{X}^{n-1})], \quad \text{(predictor step)} \\ X^{n+1} &= X^n + \tfrac{1}{2}\delta t[F(\tilde{X}^{n+1}) + F(\tilde{X}^n)], \quad \text{(corrector step)} \end{aligned}\right\} \tag{2.8}$$

where $\tilde{X}$ denotes the uncorrected value of X and the superscripts indicate the time level. The partially corrected scheme, unlike its uncorrected relative which has a weak instability with amplification factor $1+O(\delta t^2)$, is stable provided the CFL criterion is satisfied. A fully corrected scheme also exists which is slightly more accurate than (2.8), although all two-level Adams–Bashforth schemes are formally of second-order accuracy. However, the fully corrected scheme requires the evaluation of both $F(\tilde{X})$ and $F(X)$ at every timestep whereas in (2.8) only $F(\tilde{X})$ is needed (Gazdag 1976).

The diffusive terms were treated implicitly or explicitly depending on timestep considerations. In general, explicit schemes are easily implemented but may require excessively small timesteps for numerical stability. Implicit schemes, on the other hand, have no timestep requirement for stability (unconditionally stable) but are more cumbersome to implement since typically they involve the inversion of a differential operator. Therefore we found it useful to include both schemes in our program and to let the program itself select the most advantageous at the beginning of each run. If an explicit scheme was chosen it was implemented as for the advective terms above. Alternatively an implicit Crank–Nicolson scheme (see, for example, Richtmyer & Morton 1967) was employed which, for the diffusive term in (2.7), takes the form

$$X^{n+1} = X^n + \tfrac{1}{2}\delta t[D(X^{n+1}) + D(X^n)].$$

It can be seen from the last equation that, in this case, the inversion of a parabolic operator is required.

In order to carry out the programme outlined above F and D must be calculated from X and $\boldsymbol{u}$ at every timestep. For the full system of equations (2.1)–(2.5) this requires the evaluation of products of field variables together with their first- and second-order spatial derivatives. Because of the periodicity in the horizontal direction it is natural to represent the field variables by Fourier expansions in x. Horizontal derivatives are then calculated in phase space where they reduce to simple multiplications by powers of the wavenumbers. Derivatives in the vertical direction were represented by fourth-order finite differences thereby allowing for an easy treatment of the boundary conditions at $z = 0, 1$. Nonlinear terms which require products of field variables are best calculated in configuration space thus avoiding the heavy numerical burden of evaluating convolution sums. Of course, since the variables are transformed between phase space and configuration space several times per iteration, this technique, normally referred to as a pseudospectral method (Gottlieb & Orszag 1977), requires a very efficient fast Fourier transform.

3. Instabilities of the static initial state

3.1. *The linear regime*

As expected from the physical characteristics of the problem, for small values of τ the onset of instability is via an exchange of stabilities. We find that there is always one dominant unstable mode which grows appreciably before any of the harmonics lose stability – this is fortunate since it makes the task of selecting the desired mode out of the $5n$ possible eigenfunctions a relatively simple one. As required for a well-posed problem, provided that τ is reasonably small ($\lesssim 0.1$), the instabilities are found to grow exponentially on a much shorter timescale than that on which the field diffuses.

Since the instability is driven by a discontinuity in the density at the upper

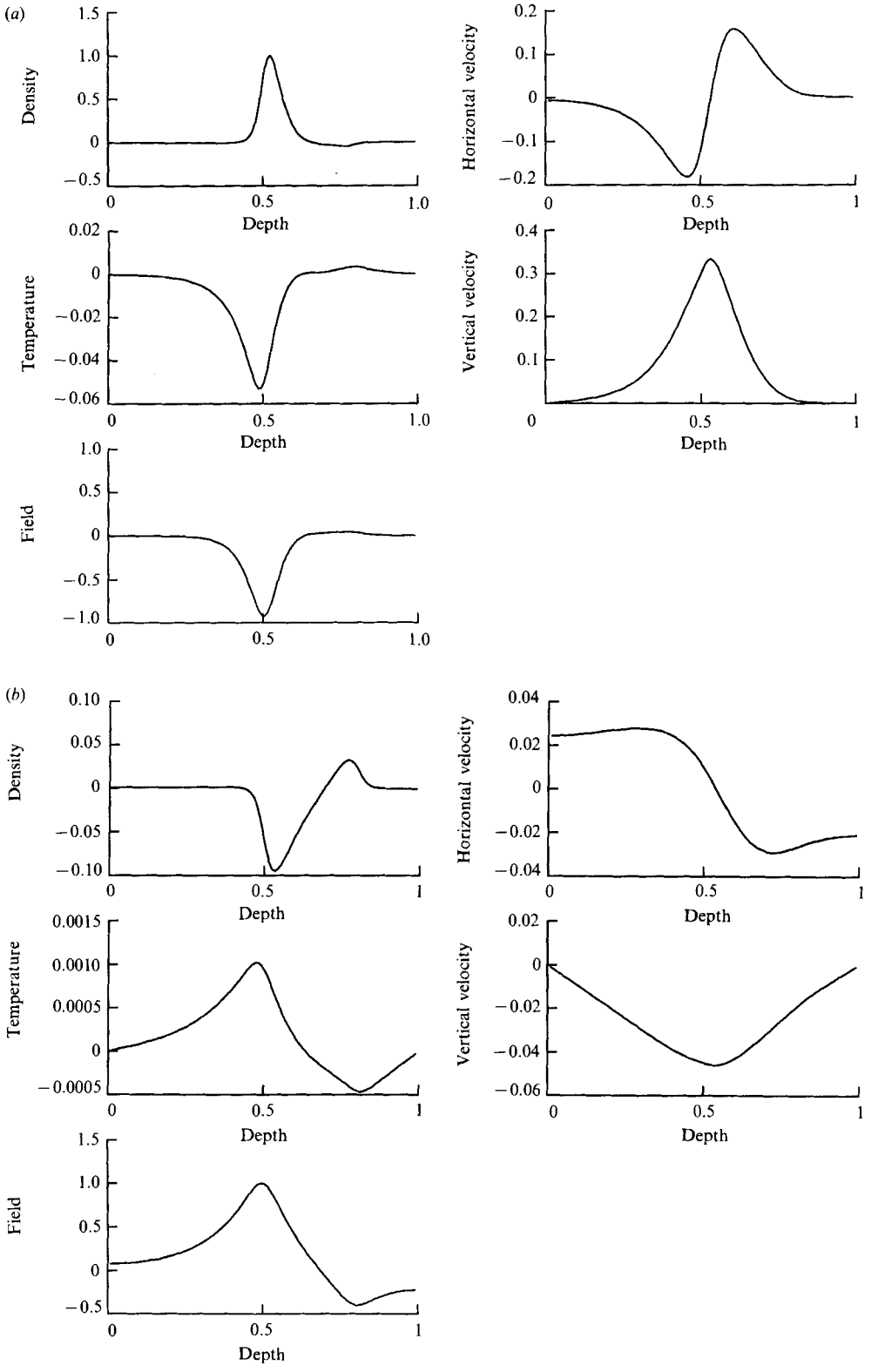

FIGURE 3. Linear eigenfunctions for the mode of maximum growth rate; in (*a*) the atmosphere is strongly stratified ($\theta = 2, \beta_\ell = 2$); in (*b*) the stratification is weaker ($\theta = 0.3, \beta_\ell = 10$). In (*a*) $\tau = 0.1$, in (*b*) $\tau = 0.05$. For both cases $\gamma = \frac{5}{3}$, $m = 1.6$, $\sigma = 0.1$, $C_k = 0.05$, $z_1 = 0.5$, $z_2 = 0.8$. The horizontal wavenumbers for (*a*) and (*b*) are 11 and 4 respectively.

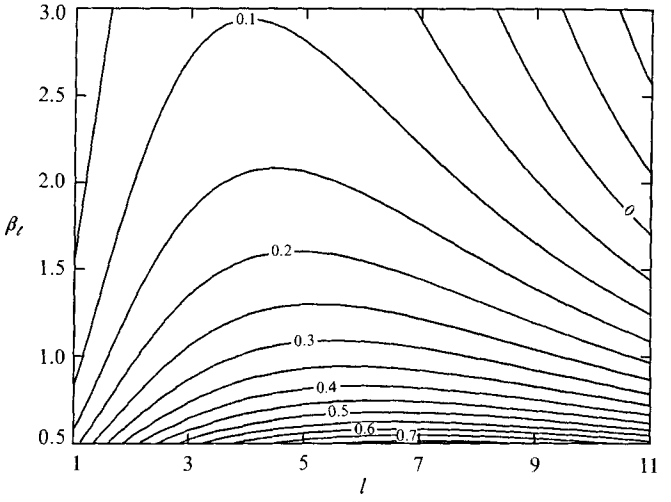

FIGURE 4. Contour plot of the growth rate as a function of β_ℓ and horizontal wavenumber l. $\gamma = \frac{5}{3}$, $m = 1.6$, $\theta = 0.1$, $\sigma = 0.1$, $\tau = C_k = 0.05$, $z_1 = 0.5$, $z_2 = 0.8$.

interface of the magnetic field it is not surprising that the eigenfunctions are peaked in this region (see figure 3). From the continuity equation (and confirmed by figure 3), associated with the peak in the vertical velocity will be a rapid change in the horizontal velocity u. As we shall see in §3.2, this horizontal shear flow centred on the upper boundary of the magnetic field has a strong influence on the subsequent nonlinear development of the instability. A wide-ranging exploration of parameter space (though keeping τ small) reveals no drastic change in the general form of the eigenfunctions. However, as is to be expected, in the magneto-Boussinesq limit of a weak field ($\beta \gg 1$) and a small temperature gradient ($\theta \ll 1$), when the jump in the density is small and the atmosphere is only weakly stratified, the eigenfunctions become less sharply peaked about the magnetic-field boundary and instead vary more gently over the entire vertical domain. This is illustrated by comparison of figures 3(*a*) and 3(*b*).

As shown by the contour plot of figure 4, decreasing β (increasing the magnetic-field strength) both increases the growth rate and also moves the mode of maximum growth rate towards larger l (narrower cells). In the absence of all diffusion the growth rate is maximized for infinitesimally thin cells ($l \to \infty$); however, dissipation acts most effectively on such cells and therefore the mode of maximum growth rate becomes of finite size. For small values of β the instability is sufficiently strong that diffusive effects are relatively weak and therefore the fastest-growing cells are quite narrow; at larger β the instability is less vigorous, the effects of diffusion are more important and thus the mode of maximum growth rate becomes wider. It should also be noted that in either of the limits $\beta \to 0$ (strong field) or $C_k \to 0$ (vanishing dissipation) the curve of maximum growth rate as a function of l becomes flatter. This implies that instability can occur for a broad band of wavenumbers, a feature that has important consequences in the nonlinear regime. Analogous results are found in the standard Rayleigh–Taylor instability of two superposed viscous fluids (Chandrasekhar 1961, §94).

A more surprising feature of this linear instability is that the mode of maximum growth rate has only a weak dependence on h, the depth of the magnetic region. This

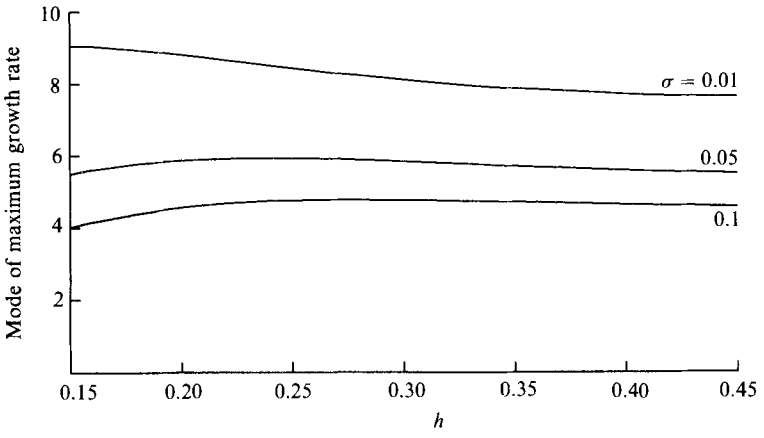

FIGURE 5. Mode of maximum growth rate as a function of the depth of the magnetic layer, h. $\gamma = \frac{5}{3}$, $m = 1.6$, $\theta = 0.5$, $\beta_\ell = 10$, $\tau = C_k = 0.05$, $z_1 = 0.5$. The Prandtl number σ is as shown.

is illustrated by figure 5 which plots the mode of maximum growth rate versus h for three different values of the Prandtl number. The mode of maximum growth rate appears to be determined primarily by striking a balance between the destabilizing influence of the density contrast at the upper interface of the magnetic field and the stabilizing dissipative effects. Only when the magnetic layer is very thin is the full extent of the layer felt – in such cases the instability is weak and the mode of maximum growth rate moves to wider cells to minimize the viscous forces.

It is of interest to compare our linear results with those obtained by Spruit & van Ballegooijen (1982) who studied the superficially similar problem of the stability of an isolated horizontal flux tube. They found that for disturbances that do not bend the tube instability can occur only if the external (non-magnetic) medium is superadiabatically stratified and that, in such cases, increasing the strength of the magnetic field within the tube is stabilizing. By contrast, in our model instability can occur for subadiabatic (and superadiabatic) atmospheres and the effect of increasing the magnetic-field strength is to enhance the instability, as illustrated in figure 4. These fundamental differences in behaviour reflect important differences in the initial states of the two models. In order for an isolated flux tube to be in static equilibrium with its surroundings (i.e. with the same density and total pressure) it must necessarily be cooler than the adjacent non-magnetic gas and consequently, in order to maintain equilibrium, increasing the strength of the magnetic field just has the indirect effect of making the tube cooler. When the tube is perturbed from equilibrium its total pressure variation is accounted for by changes in both the gas pressure and magnetic pressure. As the field strength is increased the latter becomes dominant and, as may easily be verified by a parcel argument, the density variation of the tube becomes small – since the external atmosphere is unaffected by changes in the field strength of the tube this is therefore stabilizing. The situation for a magnetic layer, on the other hand, is markedly different since the initial equilibrium state is completely independent of the horizontal direction and thus no cooling of the magnetic region is required. Any increase in the field strength simply renders the gas more top-heavy and hence more susceptible to instability.

3.2. *The nonlinear regime*

Small disturbances of the static top-hat initial state described in §2 are used as initial conditions for the fully nonlinear calculations, the subsequent nonlinear evolution being determined by (2.1)–(2.5). We have looked at several different cases, concentrating on variations in the magnetic field intensity (altering β) and in the stratification of the initial atmosphere (altering θ). In our computations σ, τ and C_k were always small ($\ll 1$) and the atmosphere always subadiabatically stratified ($m > 1/(\gamma-1)$). Although, as predicted by linear theory, variations in β and θ lead to differences in both the growth rate and the preferred horizontal scale of the instability, the general form of the instability is qualitatively unchanged. In this section we present the results from two of our calculations. If the initial state is perturbed in a quite random manner then the resulting nonlinear evolution is fairly complicated. Such an example is dealt with in the latter part of this section, but first we shall consider a simpler case which serves to illustrate many essential features of the instability.

Although the simplest case we could study is that of a single-humped disturbance in the horizontal direction, the symmetry of this perturbation means that interesting interactions between modes of different amplitude do not occur. In order to include the competition between different modes we have therefore considered the simplest asymmetrical disturbance, the initial perturbation having two humps of slightly differing amplitudes. The nonlinear evolution of the instability is portrayed in figure 6 (plate 1), which shows four important properties of the flow at selected timesteps. The upper left picture allows the magnetic field (pointing out of the paper); the lower left the vorticity (positive vorticity corresponding to anticlockwise motions); the lower right shows $\delta\rho$, the density fluctuations about the horizontal mean; the upper right the buoyancy work, the product of w and $\delta\rho$ (positive buoyancy work corresponding to light gas moving up or heavy gas moving down, negative buoyancy work to light gas moving down or heavy gas moving up). The parameter values for this calculation are $\sigma = 0.01$, $\tau = 0.01$, $\gamma = \frac{5}{3}$, $m = 1.6$, $\theta = 2.0$, $C_k = 0.05$, $\beta = 1.0$ ($\beta_\ell = 7.77$); $z_1 = 0.6$, $z_2 = 0.8$; N_x, the number of Fourier modes in the horizontal direction, is 128; N_z, the number of grid points in the vertical is also 128; the aspect ratio of the computational domain is 1.

As illustrated in figure 7, after an initial decline resulting from the starting perturbation, the kinetic energy grows rapidly owing to the release of the gravitational potential energy stored by virtue of the magnetic field. The magnetic field rises and expands, causing a shearing motion along the interface between the magnetic field and the field-free gas, as predicted by the linear eigenfunction (figure 3). The question of whether this shear can excite secondary Kelvin–Helmholtz instabilities is an important one with a tremendous bearing on the subsequent motion. If the density contrast between the light and heavy gases is small then Kelvin–Helmholtz instabilities are easily excited (see, for example, Chandrasekhar 1961, §101), regions of concentrated vorticity are formed and the unstable interface is mushroom-shaped. This is the case illustrated in figure 6 where the ratio of the density in the magnetic gas to that in the field-free gas above is $1-0.5\beta_\ell^{-1}$ ($= 0.94$). If, on the other hand, there is a substantial discrepancy between the densities of the heavy and light gases then Kelvin–Helmholtz instabilities are suppressed and the development of the unstable interface is controlled principally by inertial effects. The heavy falling gas meets little resistance and forms long narrow spikes; in contrast, the rising, less dense gas finds it difficult to accelerate into the denser gas

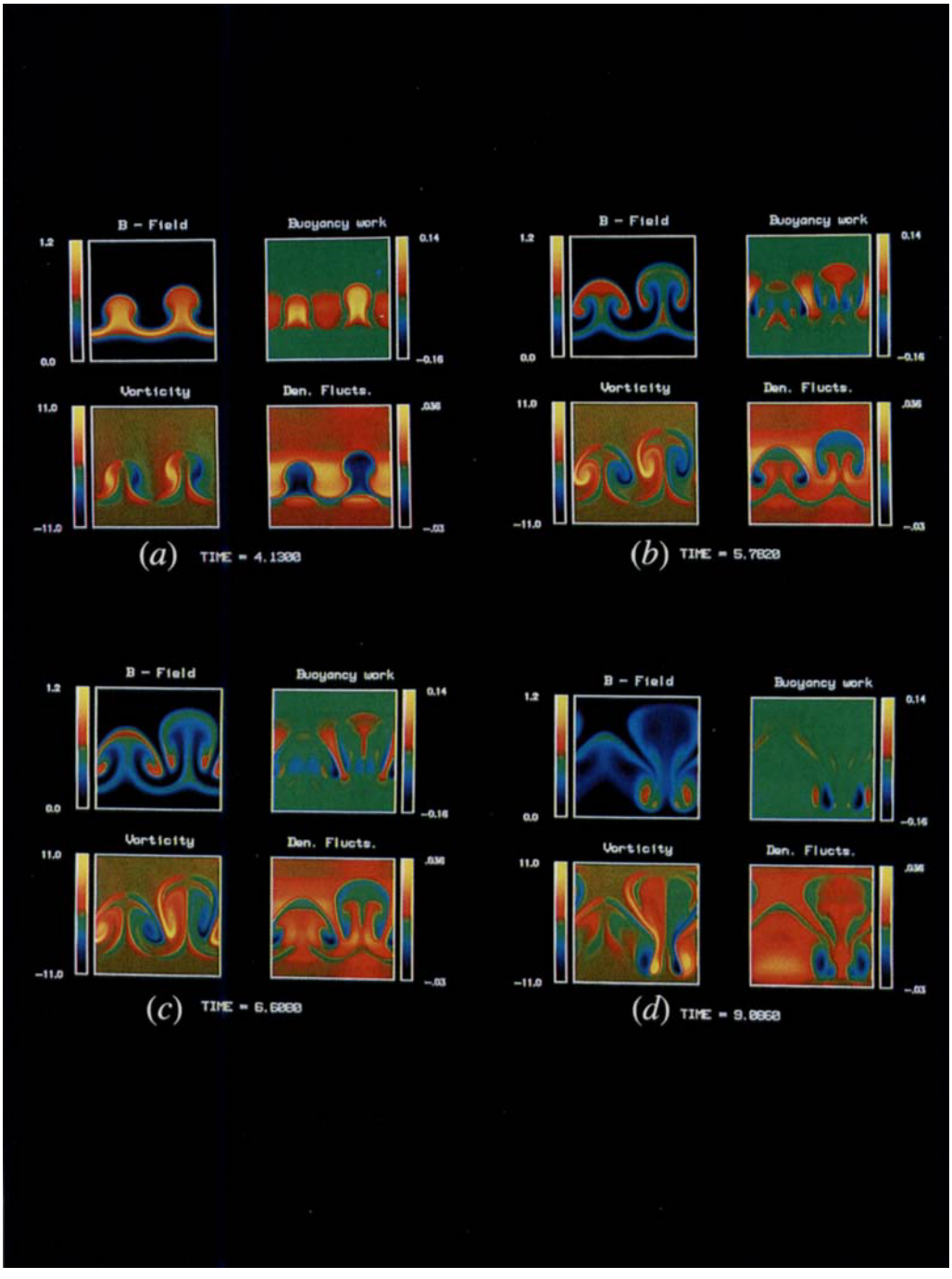

FIGURE 6. Four phases of the evolution of the two-mushrooms instability. $\gamma = 5/3$, $m = 1.6$, $\theta = 2$, $\beta = 1$, $\sigma = \tau = 0.01$, $C_k = 0.05$, $z_1 = 0.6$, $z_2 = 0.8$.

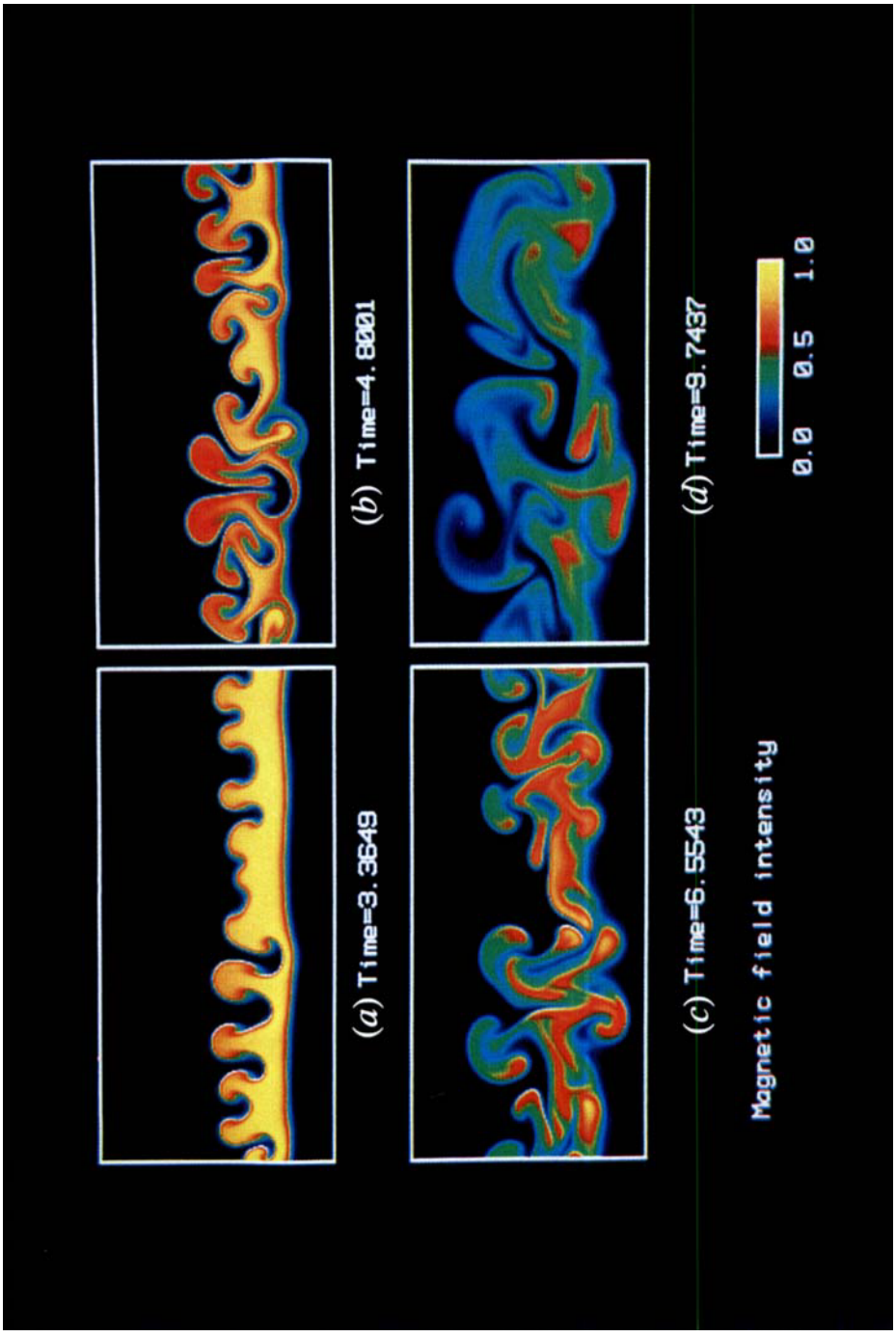

FIGURE 8. Evolution of the magnetic field for the instability started from random initial conditions. $\gamma = 5/3$, $m = 1.6$, $\theta = 2$, $\beta = 1$, $\sigma = 0.1$, $\tau = 0.01$, $C_k = 0.01$, $z_1 = 0.6$, $z_2 = 0.8$.

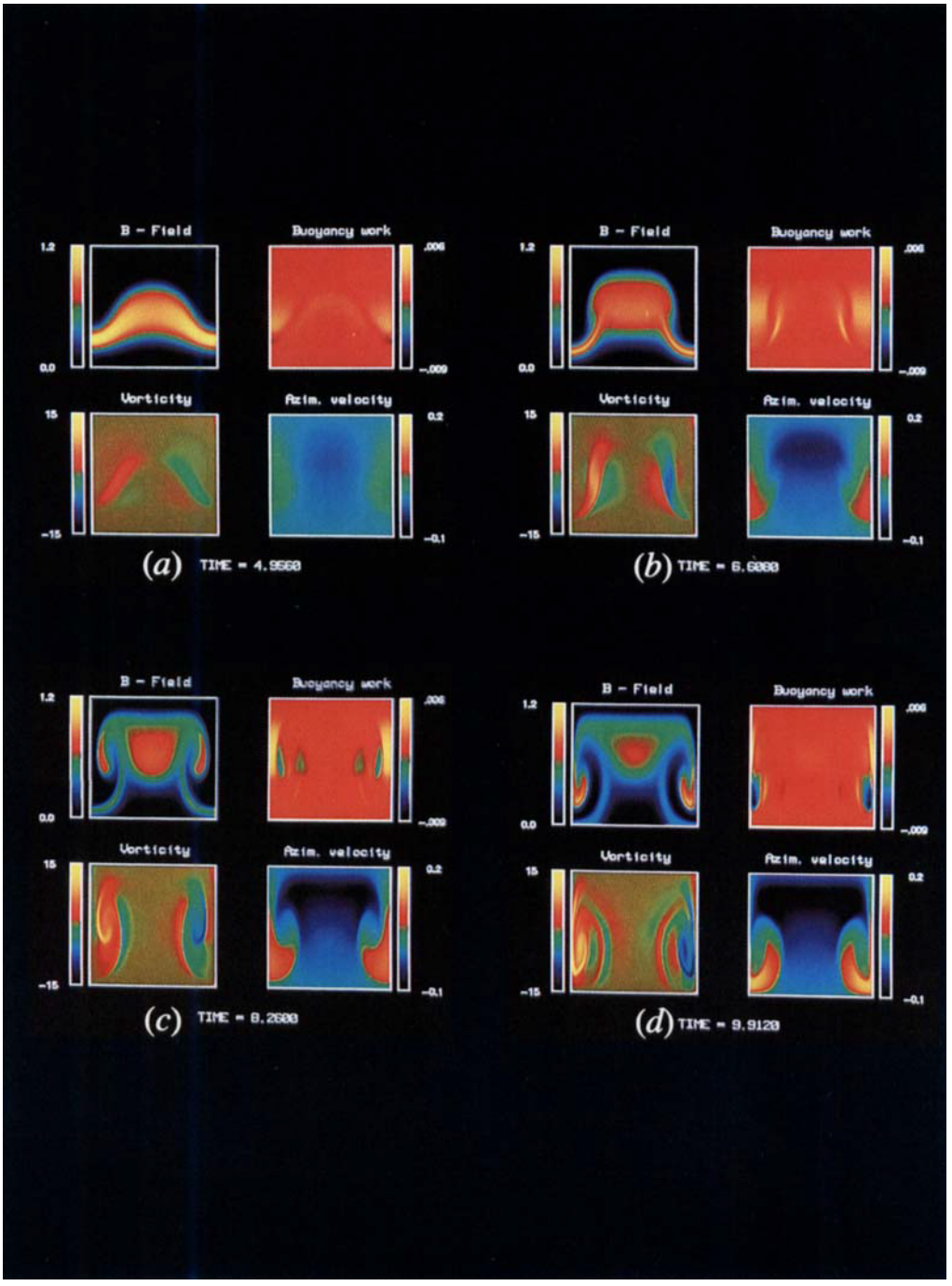

FIGURE 15. Four phases of the evolution of the single-mushroom instability incorporating rotation. $\gamma = 5/3$, $m = 1.6$, $\Omega = 0.1$, $\theta = 2$, $\beta = 1$, $\sigma = \tau = 0.01$, $C_k = 0.05$, $z_1 = 0.6$, $z_2 = 0.8$.

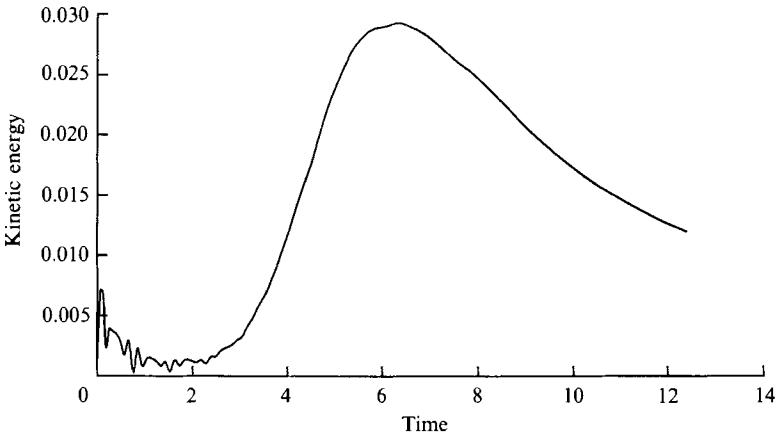

FIGURE 7. Averaged kinetic energy density as a function of time for the two-mushrooms case.

above and assumes the form of rounded bubbles (see, for instance, Daly 1967). In none of our calculations was the density contrast ever large enough for the resulting flow to enter the 'bubbles and spikes' regime.

It can be seen clearly from figure 6(*a*) that, as required for a sensible problem, the magnetic field has been distorted considerably more by the action of the instability than by diffusive processes. Whereas the instability is essentially responsible for the formation of the mushrooms, diffusion merely spreads out the magnetic field slightly at the interface with the field-free gas.

By the time $t \approx 6$ it can be seen from figure 7 that the kinetic energy has ceased to grow, and it is at this stage that there is a change in the character of the problem. Whereas initially the dynamics is controlled by the rising of the magnetic gas and the creation of regions of strong vorticity, in the latter stages, when most of the available potential energy has been released, it is the interaction between these vortices that becomes the most important feature of the flow. In general, the problem of several interacting vortices is fearsomely complicated; however, for the instabilities we are considering, the dominant interactions are pairwise between vortices on neighbouring mushrooms, which simplifies matters considerably. It is well known (see, for example, Lamb 1932, §155) that two vortices moving under their mutual interaction remain the same distance apart and move about their common centre of vorticity, a special case of this being that two vortices of equal strength but opposite sign move in a straight line perpendicular to the line joining them. The neighbouring vortices on the mushrooms of figure 6 are of opposite sign and of comparable (though not exactly equal) magnitude and so behave approximately in this manner. (It may also be noted that, owing to the assumption of periodic boundary conditions, there is a similar interaction between the outermost vortices of both mushrooms.) The feature of most interest is that the vortices are spinning so as to move downwards and, as a consequence, patches of high magnetic field can be trapped towards the bottom of the layer, even though such regions are lighter than their surroundings and would, in the absence of any other flow, rise. This point is clearly illustrated in figure 6(*b*, *c*) which shows the correspondence between regions of high magnetic field at the tips of the mushrooms and regions of negative buoyancy work. These pairwise vortex–vortex interactions persist, thereby trapping small pockets of magnetic field for long periods of time; even when $t \gtrsim 9$ (figure 6*d*) and most of the field of the

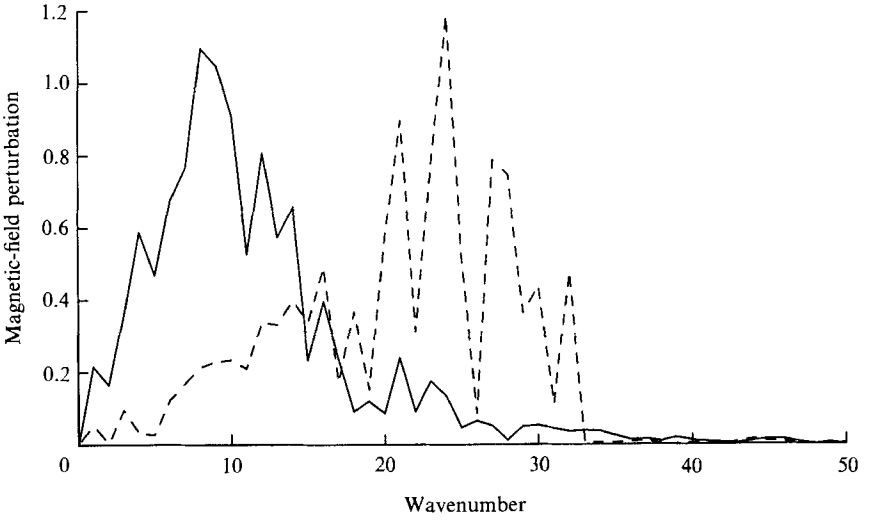

FIGURE 9. The intensity of the magnetic-field perturbation at the upper interface ($z = 0.6$) as a function of wavenumber at two different times; $t = 2.065 \times 10^{-2}$ (dashed line), $t = 2.29$ (solid line).

upper mushroom has been dispersed there remain two small areas where the field strength is still greater than half of its initial value. Close inspection of these regions reveals that most of the field has come from the tips of the lower mushroom with only a small fraction from the wings of its taller neighbour – the reason why in figure 6 (*d*) they both appear on the right-hand side of the computational domain is that the smaller mushroom has expanded horizontally and one tip, having moved out of the left-hand side, has promptly reappeared on the right to satisfy the periodic boundary conditions.

Having identified the key physical mechanisms by the relatively simple example above we can now see them in action in a more realistic calculation started from random initial conditions. The evolution of the magnetic field is portrayed in figure 8 (plate 2), the parameter values being as for the two-mushrooms calculation just described except that $\sigma = 0.1$ and $C_k = 0.01$; for this run $N_x = 256, N_z = 120$ and the aspect ratio is 2. The instability was triggered by a small perturbation in the temperature field consisting of the random superposition of waves with wavenumbers between 16 and 32. Unlike in the previous calculation, the amplitude of the initial disturbance was chosen to be sufficiently small (0.05) to allow the preferred horizontal scale to emerge dynamically.

The initial phase is characterized by the exponential growth of the kinetic energy and by the formation of small undulations on the upper interface. The wavelength of these undulations agrees well with the predictions of linear theory; for example, in this particular case, the mode of maximum growth rate has horizontal wavenumber $l \approx 33$ which corresponds to 10 peaks in our domain. Since it is these undulations that give rise to the mushrooms which persist throughout most of the evolution, linear theory provides a reliable indication of the preferred horizontal scales even in the nonlinear regime. This is exemplified by figure 9 which illustrates the intensity of the magnetic-field perturbation as a function of wavenumber at two different times. The earlier (dashed) curve represents the high-frequency response to the initial perturbation; the later (solid) curve reflects the evolution to the smaller preferred

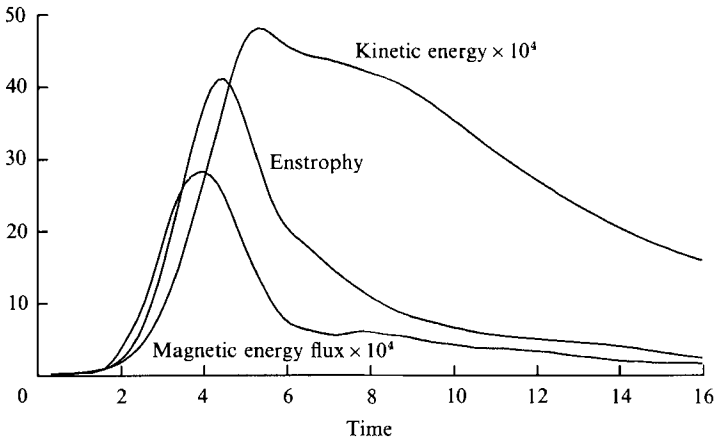

FIGURE 10. Averaged kinetic energy density, enstrophy and magnetic energy flux as a function of time.

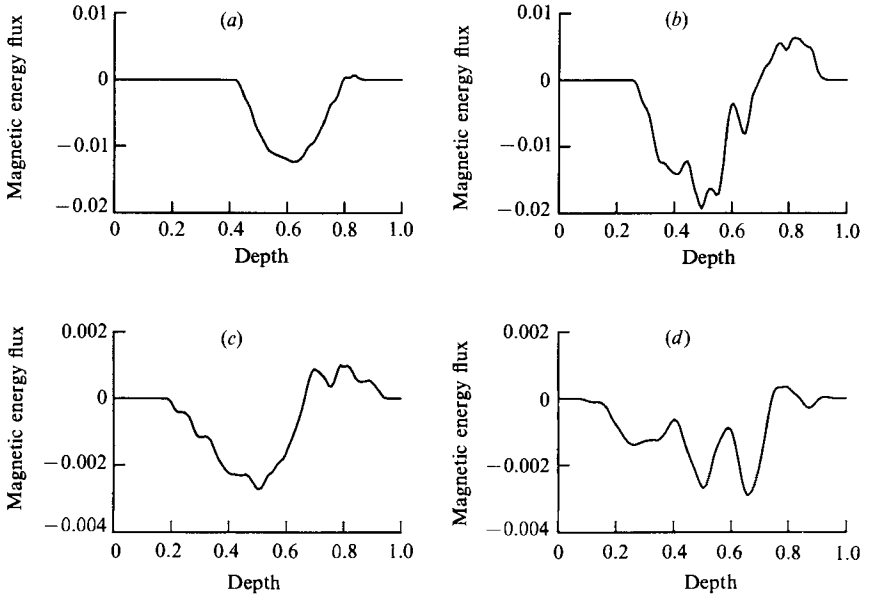

FIGURE 11. Magnetic energy flux as a function of depth at four different times. (*a*) $t = 4.0027$; (*b*) 6.0759; (*c*) 7.0327; (*d*) 10.063.

wavenumbers. The foregoing considerations should be qualified by recalling from §3.1 that as $\beta C_k \to 0$ the growth rate depends only weakly on wavenumber and therefore in this limit the selection of a preferred horizontal scale will be influenced more by the initial conditions.

As the amplitude of the perturbation grows the familiar mushrooms begin to form but, because of the randomness in the initial conditions, the outgrowths are rather more irregular. Associated with the range in mushroom size is a corresponding range in the intensity of the vortices formed at the tips of the mushrooms. One consequence of this is that since, typically, any mushroom's two neighbours will be of different sizes the vortex–vortex interactions quickly destroy the symmetry of the mushrooms. This can be seen clearly in figure 8(*b*, *c*) which shows how the field

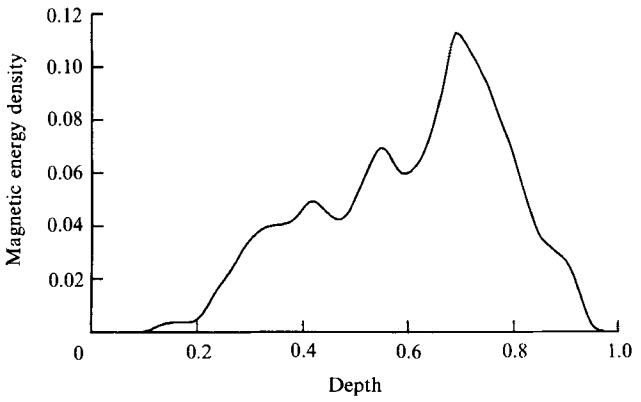

FIGURE 12. Horizontally averaged magnetic energy density as a function of depth at $t = 8.9464$.

rapidly becomes distorted. The relation between the formation of mushrooms and regions of intense vorticity and their dynamical influence is illustrated by figure 10 which plots the evolution of the enstrophy, kinetic energy and magnetic energy flux. Until $t \approx 4$ all three quantities increase; the subsequent rapid decline of the magnetic energy flux is due not to the instability running out of steam, as evinced by the still rising kinetic energy, but to the overwhelming influence of vortex–vortex interactions. Indeed, as already mentioned, these interactions can be so strong as to cause the downward displacement of regions of intense magnetic field as shown both by the behaviour of the two large mushrooms in the centre-left of figure 8(*b*, *c*) and by the appearance of positive magnetic energy flux in figure 11.

The final stages of the instability are controlled primarily by diffusion, spreading the magnetic field throughout the entire domain, and by a slow rundown of the motions by viscous processes. For times long compared with the growth time of the instability but short in comparison with the Ohmic diffusion time (figure 8*d*), the magnetic field is heavily fragmented but, because of the effects of vorticity, the peak magnetic-energy density occurs in the neighbourhood of z_2, the base of the initial magnetic layer (see figure 12).

4. Incorporating the effects of uniform rotation

Given the particular astrophysical motivation for the problem we have studied it is only natural to give some thought to the effects of rotation on the instability. In general, the incorporation of rotation into a magnetic system leads to several new wave-like modes which have fully three-dimensional motions (see, for example, Acheson & Hide 1973) and which therefore fall outside the range of our present study. In this section we shall confine ourselves to considering the influence of rotation on the interchange modes of §3, although of course being fully aware that other, possibly more important, modes have been omitted. In order to make the effects of rotation more apparent we found that it was necessary to consider rather rapid rotation rates, somewhat faster than that of the sun.

4.1. *The linear regime*

The interchange modes of §3 can be thought of as the axisymmetric exchange of rings of fluid. In the absence of magnetic fields, a simple argument making use of the conservation of angular momentum when two rings of fluid are exchanged leads to

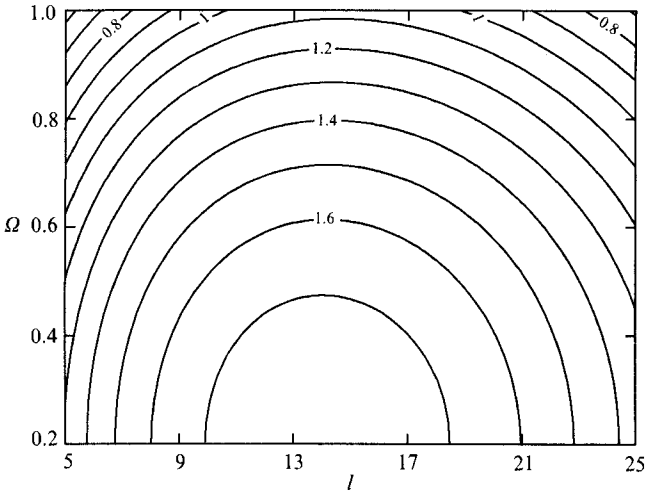

FIGURE 13. Contour plot of the growth rate as a function of Ω and horizontal wavenumber l. $\gamma = \frac{5}{3}$, $m = 1.6$, $\theta = 2$, $\beta_\ell = 2$, $\sigma = 0.1$, $\tau = C_k = 0.05$, $z_1 = 0.5$, $z_2 = 0.8$

Rayleigh's criterion that a system is unstable to axisymmetric disturbances if the angular momentum decreases outwards. In particular therefore, uniform rotation will have a stabilizing influence on the direct modes of §3 – this is illustrated by the contour plot of figure 13. The angular-momentum constraint can be relaxed by the action of viscosity which allows displaced rings of fluid to mingle more readily with their surroundings. Consequently the most suitable modes for simply annulling the stabilizing effects of rotation are those with large values of l since these diffuse angular momentum most effectively – this may be verified by adopting a highly artificial viscosity which acts only on the azimuthal component of velocity and then only in the vertical direction. As the rotation rate is increased therefore, and the instability becomes weaker, two competing effects come into play. On the one hand the mode of maximum growth rate would like to move to larger values of l to diffuse angular momentum more effectively; on the other hand, to avoid the conventional stabilizing effects of dissipation, modes with smaller values of l are preferred (as in the absence of rotation). In all the examples we have looked at (see figure 13, for example) the former effect was slightly dominant and the mode of maximum growth rate assumed a larger value of l as the rotation rate increased. It is, however, by no means apparent that this should be true in general.

When considering the instabilities arising from vertical gradients of a diffuse horizontal magnetic field, Hughes (1985*b*) showed that if $\tau \gtrsim \sigma$ instability could occur via a Hopf bifurcation. In our model, linear theory also predicts oscillatory modes, but serious problems arise when these are pursued into the nonlinear regime. The oscillatory instability is characterized by a small frequency and by again requiring that $\tau \gtrsim \sigma$. Thus the oscillatory nature of the instability is never fully realized for, if the growth rate is large, the layer is disrupted in a fraction of the period whereas, if the growth rate is small, the layer is changed appreciably by Ohmic diffusion in one growth rime. The nonlinear evolution of a layer that is predicted by linear theory to be overstable is portrayed in figure 14 where it can be seen that no oscillatory behaviour is present.

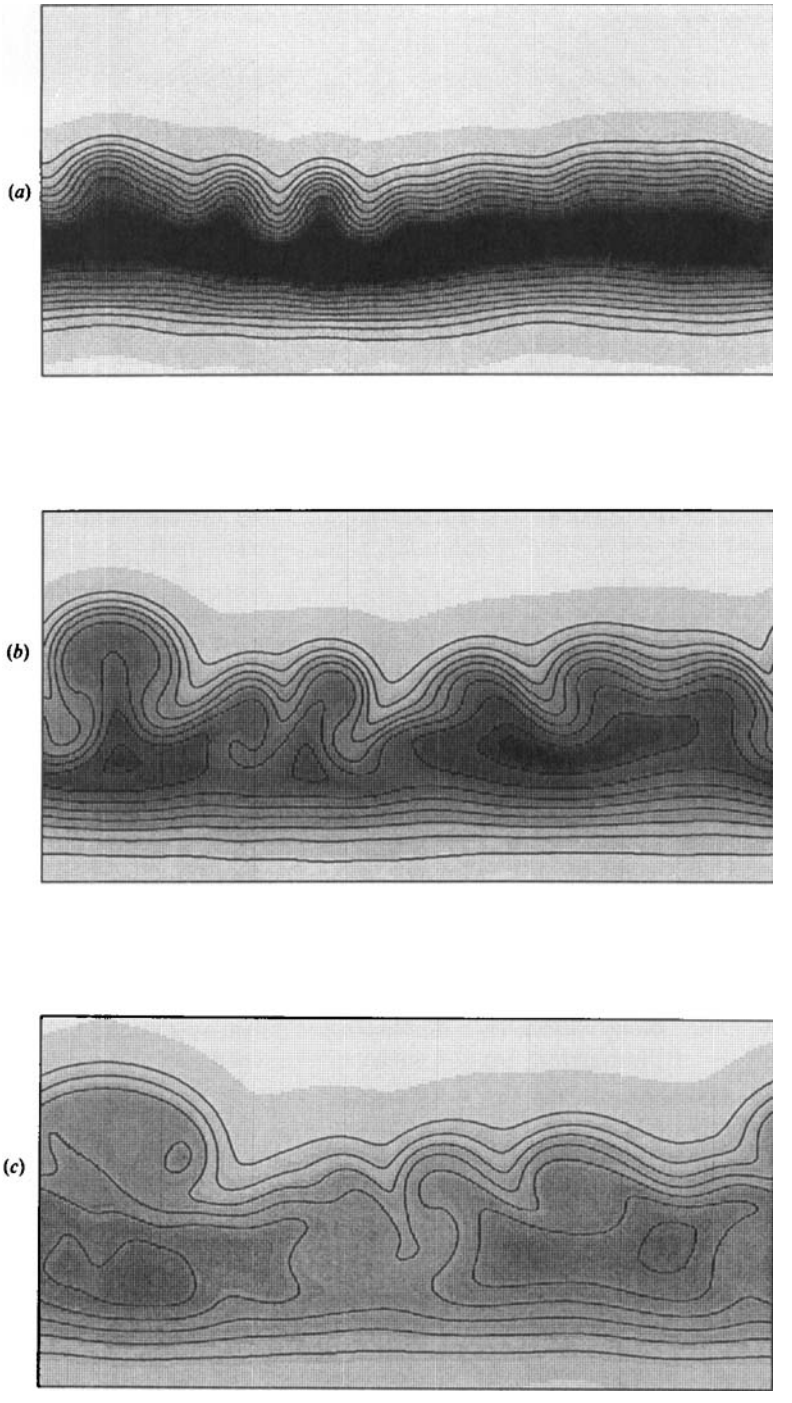

FIGURE 14. The evolution of the magnetic field for a rotating instability with random initial conditions. $\gamma = \frac{5}{3}$, $m = 2$, $\Omega = 0.15$, $\theta = 1$, $\beta = 4$, $\sigma = 0.005$, $\tau = 0.01$, $C_k = 0.05$, $z_1 = 0.6$, $z_2 = 0.8$. The aspect ratio for this calculation is 2. The times are (*a*) $t = 10.458$, (*b*) 21.912, (*c*) 34.361.

4.2. *The nonlinear regime*

Since there are many similarities between the rotating and non-rotating cases we shall here concentrate solely on the differences. These may be emphasized by studying the evolution of two rapidly rotating instabilities; from random initial conditions in figure 14 and from a simple, single-humped disturbance in figure 15 (plate 3). The parameter values for this latter calculation are the same as for the two-mushrooms case of §3.2 with a rotation rate of $\Omega = 0.1$ and an aspect ratio of 2. Figure 15 has the same layout as figure 6 except that now we have chosen to illustrate the azimuthal velocity, a feature peculiar to the rotating instability.

Owing to the powerful rotational constraint, which inhibits vertical motions, the overall evolution of the instability is more sluggish. This may be seen by a cursory inspection of figure 14 and by comparison of figures 6 and 15 which shows the instability of the static state to be progressing much faster than its rotating counterpart. Furthermore, the secondary Kelvin–Helmholtz instability, which is chiefly responsible for the formation of localized vortices in the non-rotating case, is also severely impeded by rotation (Chandrasekhar 1961, §105) and, as a result, the mushrooms of §3 become the amorphous blobs of figures 14 and 15. Consequently, since the nonlinear disruption of the layer is caused primarily by vortex–vortex interactions, the presence of weaker vortices allows the layer to remain intact for long times.

Incorporating rotation induces an azimuthal velocity which, in figure 15, is comparable in magnitude with the meridional flows. The influence of the Coriolis force can be seen clearly, with the fluid in the rising magnetic blob acquiring retrograde motion (v negative) and the descending field-free fluid between blobs moving in the opposite direction.

5. Discussion

The most important result to emerge from our calculations is that the development of the instability proceeds in two fairly distinct stages. In the first, motions are driven by the release of gravitational potential energy – the interface separating the magnetic field and the field-free gas becomes mushroom-shaped and there is a buildup of vorticity in the tips of the mushrooms. Such behaviour is not uncommon in situations involving the relative accleration of fluids (or gases) of comparable density. Two other examples illustrating this phenomenon are the injection of one fluid into another (see Batchelor 1967, plate 20), and the fragmentation of an isolated flux tube rising through a non-magnetic gas (Schüssler 1979). In the second stage there is a change in the dominant driving feature of the instability with the motion being controlled primarily by the interactions between vortices of opposite sign on neighbouring mushrooms. Other numerical simulations of Rayleigh–Taylor instabilities have not been carried beyond the preliminary stage and so this later development has not previously been observed. The interactions between vortices of different intensities lead to a rapid disruption of the layer in a time short compared with the magnetic diffusion time and, in the final stages of our calculations (see figures 6*d*, 8*d*, 15*d*), to small pockets of strong field remaining trapped towards the bottom of the computational domain. Obviously, since there is no external supply of energy to the system, all motions will eventually cease and the magnetic field will simply become uniform under the action of magnetic diffusion. It is interesting to note that, qualitatively at least, the break-up of a magnetic layer as decribed in §3

is somewhat similar to the destruction of a two-dimensional turbulent wake. Couder & Basdevant (1986) have sudied the wakes generated in thin soap films and, like us, find that a significant feature of the motion is the interactions between vortices of opposite sign (compare our figure 8 with their figure 7).

As explained in the introduction, the work of this paper was motivated by considerations of the sun's magnetic field and it is therefore important to discuss our results in that context. We cannot make any definite quantitative predictions since the dimensionless parameters of §2 take rather extreme values in the overshoot zone (for example, β is very large, σ and τ very small) and it is just not possible to perform our numerical calculations with these values. However, we do feel that the qualitative features of the instability we have described will be reproduced in the sun since, although we have overestimated the density contrast between the magnetic and field-free regions, thereby exaggerating the instability, we also have considerably more stabilizing dissipation. Thus it certainly appears that any strong toroidal field generated beneath a field-free region will be drastically distorted by magnetic Rayleigh–Taylor instabilities and that, as pointed out in §3.2, since the density contrast is small, a key role is played by the vorticity. Whether isolated flux tubes are the natural upshot of these instabilities is still unclear. The caps of the magnetic mushrooms could be thought of as the initial formation of flux tubes, but in our calculations the stems of the mushrooms were never pinched off and the strong vortex interactions prevented the rise of these features. Of course, in the sun, the region overlying the magnetic field is neither initially static nor stably stratified, as in our model, but is instead a region of turbulent convection, a fact that could significantly affect the later evolution of the instability. Should a mushroom protrude into this region it is conceivable that the turbulent motions could snap off the stem to form an isolated flux tube endowed with a certain distribution of vorticity. This conjecture could be tested by extending our model to incorporate the effects of an overlying convectively unstable region. Furthermore, if flux tubes were indeed generated with a strong vorticity it would be instructive to include this feature in models of isolated flux tubes. The interaction between a tube with vorticity and a mean flow presumably would have an influence on the path taken by the tube as it ascended through the convection zone.

Finally we shall mention what is probably the most important extension of the work described in this paper – the study of the instability to three-dimensional disturbances. As explained in the introduction, from linear theory we expect the fastest-growing mode to have a long wavelength in the direction of the imposed field. Of particular interest though would be the subsequent *nonlinear* behaviour of the vorticity mushrooms when they have more room to manoeuvre. One can imagine new instabilities due to the shear in the y-direction as well as wrapping instabilities of the type studied by Takaki & Hussain (1984). For the rapidly rotating system of §4, we envisage that the extra degree of freedom will change the character of the instability quite dramatically. The initial phase of the instability will presumably be wave-like, but after that we would not like to mak' a guess as to what might happen.

It is a pleasure to thank Professor Juri Toomre for many stimulating discussions. This work was supported by the National Aeronautics and Space Administration through grants NSG-7511, NAGW-91 and NAG5-513 and contract NAS8-31958.

REFERENCES

ACHESON, D. J. 1978 On the instability of toroidal magnetic fields and differential rotation in stars. *Phil. Trans. R. Soc. Lond.* A **289**, 459–500.

ACHESON, D. J. 1979 Instability by magnetic buoyancy. *Sol. Phys.* **62**, 23–50.

ACHESON, D. J. & GIBBONS, M. P. 1978 Magnetic instabilities of a rotating gas. *J. Fluid Mech.* **85**, 743–757.

ACHESON, D. J. & HIDE, R. 1973 Hydromagnetics of rotating fluids. *Rep. Prog. Phys.* **36**, 159–221.

BAKER, G. R., MEIRON, D. I. & ORSZAG, S. A. 1980 Vortex simulations of the Rayleigh–Taylor instability. *Phys. Fluids* **23**, 1485–1490.

BATCHELOR, G. K. 1967 *An Introduction to Fluid Dynamics.* Cambridge University Press.

CHANDRASEKHAR, S. 1961 *Hydrodynamic and Hydromagnetic Stability.* Clarendon.

COUDER, Y. & BASDEVANT, C. 1986 Experimental and numerical study of vortex couples in two-dimensional flows. *J. Fluid Mech.* **173**, 225–251.

DALY, B. J. 1967 Numerical study of two fluid Rayleigh–Taylor instability. *Phys. Fluids* **10**, 297–307.

DALY, B. J. 1969 Numerical study of the effect of surface tension on interface instability. *Phys. Fluids* **12**, 1340–1354.

GAZDAG, J. 1976 Time-differencing schemes and transform methods. *J. Comp. Phys.* **20**, 196–207.

GILMAN, P. A. 1970 Instability of magnetohydrostatic stellar interiors from magnetic buoyancy. *Astrophys. J.* **162**, 1019–1029.

GILMAN, P. A. 1983 Dynamically consistent nonlinear dynamos driven by convection in a rotating spherical shell. II. Dynamos with cycles and strong feedbacks. *Astrophys. J. Suppl.* **53**, 243–268.

GILMAN, P. A. & MILLER, J. 1981 Dynamically consistent nonlinear dynamos driven by convection in a rotating spherical shell. *Astrophys. J. Suppl.* **46**, 211–238.

GLATZMAIER, G. A. 1985*a* Numerical simulations of stellar convective dynamos. II. Field propagation in the convection zone. *Astrophys. J.* **291**, 300–307.

GLATZMAIER, G. A. 1985*b* Numerical simulations of stellar convective dynamos. III. At the base of the convection zone. *Geophys. Astrophys. Fluid Dyn.* **31**, 137–150.

GOTTLIEB, D. & ORSZAG, S. A. 1977 *Numerical Analysis of Spectral Methods: Theory and Applications.* SIAM.

HUGHES, D. W. 1985*a* Magnetic buoyancy instabilities for a static plane layer. *Geophys. Astrophys. Fluid Dyn.* **32**, 273–316.

HUGHES, D. W. 1985*b* Magnetic buoyancy instabilities incorporating rotation. *Geophys. Astrophys. Fluid Dyn.* **34**, 99–142.

HUGHES, D. W. 1987 Finite-amplitude solutions for interchange instabilities driven by magnetic buoyancy. *Geophys. Astrophys. Fluid Dyn.* **37**, 297–343.

HUGHES, D. W. & CATTANEO, F. 1987 A new look at the instability of a stratified horizontal magnetic field. *Geophys. Astrophys. Fluid Dyn.* **39**, 65–81.

KRUSKAL, M. & SCHWARZSCHILD, M. 1954 Some instabilities of a completely ionized plasma. *Proc. R. Soc. Lond.* A **223**, 348–360.

LAMB, H. 1932 *Hydrodynamics*, 6th edn. Cambridge University Press.

LAYZER, D., ROSNER, R. & DOYLE, H. T. 1979 On the origin of solar magnetic fields. *Astrophys. J.* **229**, 1126–1137.

MENIKOFF, R. & ZEMACH, C. 1983 Rayleigh–Taylor instability and the use of conformal maps for ideal fluid flow. *J. Comp. Phys.* **51**, 28–64.

MORENO-INSERTIS, F. 1983 Rise times of horizontal magnetic flux tubes in the convection zone of the sun. *Astron. Astrophys.* **122**, 241–250.

MORENO-INSERTIS, F. 1986 Nonlinear time evolution of kink-unstable magnetic flux tubes in the convective zone of the sun. *Astron. Astrophys.* **166**, 291–305.

NEWCOMB, W. A. 1961 Convective instability induced by gravity in a plasma with a frozen-in magnetic field. *Phys. Fluids* **4**, 391–396.

PARKER, E. N. 1966 The dynamical state of the interstellar gas and field. *Astrophys. J.* **145**, 811–833.

PARKER, E. N. 1975 The generation of magnetic fields in astrophysical bodies. X. Magnetic buoyancy and the solar dynamo. *Astrophys. J.* **198**, 205–209.

RAYLEIGH, LORD 1883 Investigation of the character of the equilibrium of an incompressible heavy fluid of variable density. *Proc. Lond. Math. Soc.* **14**, 170–177; *Scientific Papers* **2**, 200–207.

RICHTMYER, R. D. & MORTON, K. W. 1967 *Difference Methods for Initial Value Problems.* Interscience.

ROBERTS, P. H. & STEWARTSON, K. 1977 The effect of finite electrical and thermal conductivities on magnetic buoyancy in a rotating gas. *Astron. Nachr.* **298**, 311–318.

ROBERTS, P. H. & STIX, M. 1972 α-Effect dynamos, by the Bullard–Gellman formalism. *Astron. Astrophys.* **18**, 453–466.

SCHMITT, J. H. M. M. & ROSNER, R. 1983 Doubly diffusive magnetic buoyancy instability in the solar interior. *Astrophys. J.* **265**, 901–924.

SCHUBERT, G. 1968 The stability of toroidal magnetic fields in stellar interiors. *Astrophys. J.* **151**, 1099–1110.

SCHÜSSLER, M. 1979 Magnetic buoyancy revisited: analytical and numerical results for rising flux tubes. *Astron. Astrophys.* **71**, 79–91.

SPIEGEL, E. A. & WEISS, N. O. 1980 Magnetic activity and variations in solar luminosity. *Nature* **287**, 616–617.

SPRUIT, H. C. & VAN BALLEGOOIJEN, A. A. 1982 Stability of toroidal flux tubes in stars. *Astron. Astrophys.* **106**, 58–66.

STOER, J. & BULIRSCH, R. 1980 *Introduction to Numerical Analysis.* Springer.

TAKAKI, R. & HUSSAIN, A. K. M. F. 1984 Entanglement of two vortex filaments. In *Turbulence and Chaotic Phenomena in Fluids* (ed. T. Tatsumi), pp. 245–249. North-Holland.

TAYLOR, G. I. 1950 The instability of liquid surfaces when accelerated in a direction perpendicular to their planes. I. *Proc. R. Soc. Lond.* A **201**, 192–196.

VAN BALLEGOOIJEN, A. A. 1982 The overshoot layer at the base of the solar convective zone and the problem of magnetic flux storage. *Astron. Astrophys.* **113**, 99–112.

WANG, Y.-M. & NEPVEU, M. 1983 A numerical study of the nonlinear Rayleigh–Taylor instability, with application to accreting X-ray sources. *Astron. Astrophys.* **118**, 267–274.

YOSHIMURA, H. 1975 A model of the solar cycle driven by the dynamo action of the global convection in the solar convection zone. *Astrophys. J. Suppl.* **29**, 467–494.